Nanoscale

PAPER

View Article Online
View Journal | View Issue

Cite this: *Nanoscale*, 2021, **13**, 10925

Single-step coating of mesoporous SiO_2 onto nanoparticles: growth of yolk–shell structures from core–shell structures†

Xiaobin Xie, * Marijn A. van Huis * and Alfons van Blaaderen*

Yolk–shell nanoparticles based on mesoporous SiO_2 ($mSiO_2$) coating of Au nanoparticles (Au NPs) hold great promise for many applications in *e.g.*, catalysis, biomedicine, and sensing. Here, we present a single-step coating approach for synthesizing Au NP@$mSiO_2$ yolk–shell particles with tunable size and tunable hollow space between yolk and shell. The Au NP–$mSiO_2$ structure can be manipulated from core–shell to yolk–shell by varying the concentration of cetyltrimethylammonium chloride (CTAC), tetraethyl orthosilicate (TEOS), Au NPs, and NaOH. The growth mechanism of the yolk–shell particles was investigated in detail and consists of a concurrent process of growth, condensation, and internal etching through an outer shell. We also show by means of liquid-cell transmission electron microscopy (LC-TEM) that Au nanotriangle cores (Au NTs) in yolk–shell particles that are stuck on the $mSiO_2$ shell, can be released by mild etching thereby making them mobile and tumbling in a liquid-filled volume. Due to the systematical investigation of the reaction parameters and understanding of the formation mechanism, the method can be scaled-up by at least an order of magnitude. This route can be generally used for the synthesis of yolk–shell structures with different Au nanoparticle shapes, *e.g.*, nanoplatelets, nanorods, nanocubes, for yolk–shell structures with other metals at the core (Ag, Pd, and Pt), and additionally, using ligand exchange with other nanoparticles as cores and for synthesizing hollow $mSiO_2$ spheres as well.

Received 24th February 2021,
Accepted 31st March 2021

DOI: 10.1039/d1nr01242h

rsc.li/nanoscale

Introduction

The scientific interest in Au based nanoparticles (NPs) has vastly increased in recent decades, due to their widespread application in various fields, such as catalysis,[1–5] biomedicine,[6–8] sensing,[9–14] and energy conversion.[15–19] Generally, the performance of Au nanoparticles (Au NPs) is dependent on various factors, like size, morphology, and type of surface ligands.[20–25] Among all strategies that have been developed to achieve a better performance of Au NPs, coating with mesoporous SiO_2 ($mSiO_2$) is one of the most popular approaches, as this can significantly enhance the colloid's stability of Au NPs, act as morphological stabilizer,[26,27] mitigate the barrier/poisoning effects from ligands for catalysis, and makes them biocompatible.[13,28–30] Several typical kinds of Au NP–$mSiO_2$ structures have been developed for various applications. They are Au NP@$mSiO_2$ core–shell NPs,[28,31] Au NP@hollow–$mSiO_2$ yolk–shell structures,[32] Janus-type structures,[33] and other complex $mSiO_2$–Au structures.[34–36]

In comparison with the core–shell and other hybrid structures, the yolk–shell structure has several advantages as discussed in several reviews.[37–40] First, the tunable hollow space between core and shell provides a faster mass transfer and less impact on the core surface during catalytic reactions.[34] Furthermore, yolk–shell particles can serve as carriers used for the transport and controlled release of drugs, which is an important strategy for cancer therapy.[41] A yolk–shell morphology also has several advantages for surface enhanced Raman scattering sensing, amongst which increased reproducibility.[42,43] Lastly, with an outer $mSiO_2$ shell, the ligands or surfactants used for the synthesis of Au NP cores can be removed more easily without inducing aggregation of the Au NPs.[26,27,32,44] During the past few years, several strategies have been developed for synthesizing Au NPs@hollow@$mSiO_2$ yolk–shell structures.[34,45] However, most of these methods are comprised of multiple steps, such as hard template methods, or do not allow morphology-controlled synthesis of the cores.[37,39,40]

Here, we report a single-step coating approach which originated from a previous protocol for synthesizing Au NRs@$mSiO_2$ core–shell NPs,[31] based on a simultaneous

Soft Condensed Matter, Debye Institute for Nanomaterials Science, Utrecht University, Princetonplein 5, 3584 CC Utrecht, The Netherlands.
E-mail: xb.xie@hotmail.com, M.A.vanHuis@uu.nl, A.vanBlaaderen@uu.nl

†Electronic supplementary information (ESI) available. See DOI: 10.1039/d1nr01242h

growth-etching mechanism, to the synthesis of Au NPs@hollow@mSiO$_2$ yolk–shell structures. Moreover, various factors that impact the growth and final structure could be controlled *via* the reaction parameters. By varying the reaction conditions, the structure of the mSiO$_2$ core–shell particles was switched between core–shell and yolk–shell. Additionally, the size of the yolk–shell particles can be easily tuned by changing the concentration of the core particles. Our experiments also show that this strategy can be adopted irrespective of the core's morphology; it is universal for all shapes of Au NPs and can be used even for preparing hollow mSiO$_2$ spheres. Using ligand exchange (*e.g.* through a very general and elegant procedure developed recently[46]), we found that the surface ligands on the NPs also influence the final structure of the resulting Au NP@mSiO$_2$ structures. Furthermore, liquid-cell TEM (LC-TEM) experiments revealed that the Au NT cores can be released easily upon mild etching creating freely diffusing NP systems inside the mesoporous silica shells. Such 'rattle-type' systems are of interest for photonic applications as well.[28,43,47]

Results and discussion

The Au nanotriangles (Au NTs) were synthesized *via* a modification of the method reported by L. M. Liz-Marzán *et al.*[48] After purification, the percentage of Au NTs having an average size of 67 nm was more than 90%, and others are mainly spheres (Fig. S1a–c†). The UV-VIS spectrum of the Au NTs (Fig. S1d†) shows that the main localized surface plasmon resonance (LSPR) band is at 669 nm. Using these Au NTs as seeds, a single-step coating method was developed which was partially based on previous work in which Au NRs can be coated by mesoporous silica layers using the ligands used for the Au NR synthesis, CTAB, as pore inducing template molecules[49] in order to produce Au NT@hollow–mSiO$_2$ yolk–shell nanoparticles. Fig. 1a shows the morphology of the yolk–shell nanoparticles having Au NT cores inside a mSiO$_2$ outer shells. The edge length of the Au NTs used for the synthesis of these yolk–shell nanoparticles was about 68 nm on average while the overall particle diameter for the particular synthesis shown in Fig. 1 was about 205 nm, where the thickness of the shell was around 33 nm (Fig. 1c). We found a weak positive correlation between the diameter of the yolk–shell particles and the edge length of the Au NT cores, and there was no correlation found between the shell thickness and the diameter of whole particles or with the edge lengths of the Au NTs (Fig. 1d).

In order to understand the effect of the reaction parameters on the morphology of the Au NT@mSiO$_2$ products, a series of control variable experiments were performed with precise tuning of the reaction conditions. First of all, we found that the concentration of CTAC plays an important role in the formation of the yolk–shell structure. We assume that all cetyltri-

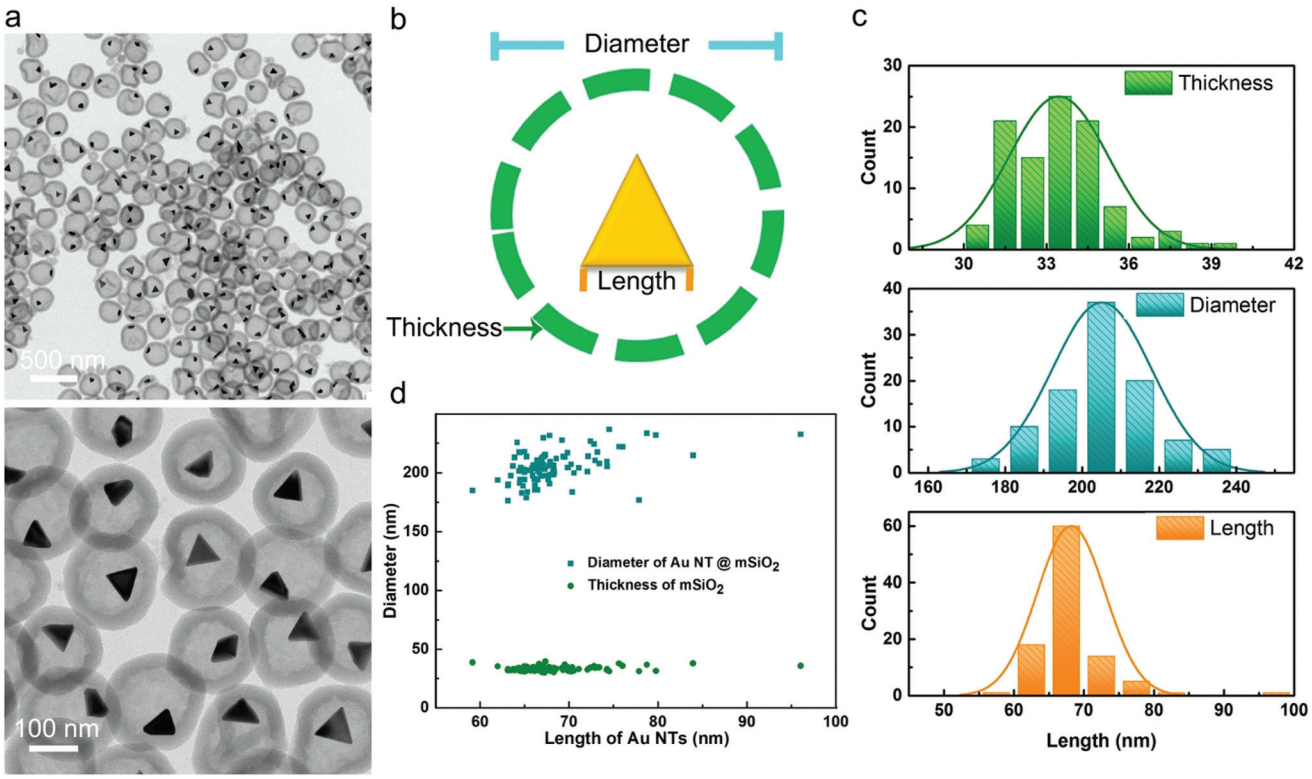

Fig. 1 (a) Bright-field transmission electron microscopy (BF-TEM) images of Au NT@hollow–mSiO$_2$ yolk–shell nanoparticles; (b) schematic of Au NT@hollow–mSiO$_2$ yolk–shell nanoparticle morphology; (c) size distribution of Au NT@hollow–mSiO$_2$ yolk–shell nanoparticles; (d) the relationship between Au NT edge length and shell thickness and diameter.

methylammonium (CAT^+) ions are forming a double layer on the surface of the Au NTs after washing and resuspension in water. The concentration of this surfactant is around the critical micelle concentration (CMC) 1.3 mM in water.[50] As shown in Fig. S2,† the morphology and structure of the Au NT@$mSiO_2$ particles changes as different amounts of additional CTAC are added to the growth solution. Au NT@$mSiO_2$ core–shell particles were formed both at low (≤0.5 mM) and relatively high (≥3.0 mM) concentrations as compared to the CMC value of 1.3 mM.[50] When the concentration of additional CTAC was between 1.0 mM to 2.0 mM, Au NT@hollow–$mSiO_2$ yolk–shell particles were obtained. Moreover, both the way of injecting TEOS and the amount of TEOS was found to influence the final structure of the particles. Fig. S3† indicates that 200 μl of 20 vol% TEOS (in methanol) injected separately into three shoots lead to a core–shell structure. Also 200 μl injections in one shot of 15 vol%, 10 vol%, and 5 vol% TEOS resulted in core–shell Au NT@$mSiO_2$ particles (Fig. 2).

To investigate the influence of the number of Au NTs cores, different concentrations of Au NTs were used for the yolk–shell synthesis. As shown in Fig. 3, the TEM images indicate that the hollow space in the Au NT@hollow–$mSiO_2$ yolk–shell particles was reduced when the concentration of Au NTs increases from 112 pM to 900 pM (Fig. 3a). The diameters and shell thicknesses of the Au NT@$mSiO_2$ yolk–shell particles obtained using different concentrations of Au NTs were determined by averaging the dimensions of more than 100 yolk–shell particles in the acquired TEM images. The average diameters of the yolk–shell particles were 210 nm, 175 nm, 145 nm, and 120 nm, decreasing with increasing Au NT concentration (Fig. 3b and d). This trend was also observed for the shell thickness, although it changed only slightly. The four $mSiO_2$ shell average thicknesses were 33 nm, 32 nm, 30 nm, and 29 nm, respectively. Notably, secondary nucleation of silica particles was only observed when the concentration of Au NTs was 112 pM. Fig. 3d and e show the relationship between Au NT concentrations and diameters and shell thickness, the bars in the bar graphs are providing the min–max range, the block center indicates the average size, and the block range denotes the standard deviation. Furthermore, we studied the effect of the surface ligands on the synthesis *via* ligand exchange. The CTA^+ double layers on the Au NT surface were exchanged by other ligands that have been commonly used for noble metals nanoparticles synthesis or surface decoration. They are CTAB, PEG–SH, and PVP, respectively.[51] The UV-VIS spectra of the Au NTs with different ligands recorded after ligand exchange indicate that the Au NTs were still well dispersed in water except for the Au NTs coated by-PVP where the particles were slightly aggregated (Fig. S5†). It is not surprising that Au NT-CTAB form Au NT@hollow–$mSiO_2$ yolk–shell structures similarly to those obtained with Au NT-CTAC (Fig. S6a†), considering that the same CTA^+ ions double layers are covering the Au NTs surfaces. However, $mSiO_2$ shells failed to grow on Au NT–PEG–SH and Au NT–PVP surfaces, and consequently growth of hollow *empty* $mSiO_2$ nanospheres (NSs) was found instead (Fig. S6b and c†).

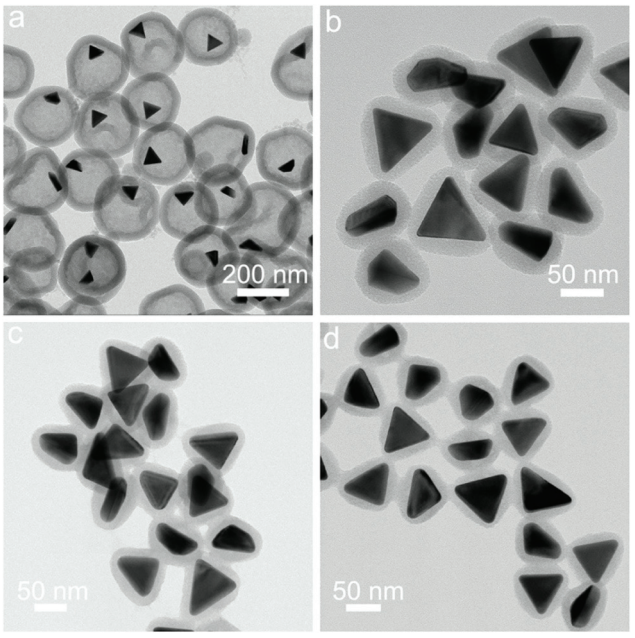

Fig. 2 Influence of the concentration of TEOS on the morphology of the Au NT@$mSiO_2$ structures. Here the concentrations of TEOS precursor solution used for the reaction were: (a) 20 vol%, (b) 15 vol%, (c) 10 vol%, and (d) 5 vol%.

To elucidate the formation mechanism of the Au NT@hollow–$mSiO_2$ yolk–shell structures, we monitored the growth process in time by recording TEM images at various stages of the growth process. The reaction was stopped by centrifugation after specific reaction times after which TEM grids were prepared. Fig. 4a shows the shape evolution of the Au NT@$mSiO_2$ particles. After the first 20 min, $mSiO_2$ shells are seen to have grown on the Au NTs' surfaces. In the second stage, $mSiO_2$ shells became visible, accompanied by etching of the $mSiO_2$ silica interior, which occurred from 20 min to 80 min. Subsequently, etching of $mSiO_2$ became the dominant process in the next stage until a well-defined 'yolk–shell' Au NT@mSO_2 morphology was obtained. This growth-etching mechanism can be summarized as shown in the schematic in Fig. 4b. The sol–gel reactions for the growth and etching processes can be expressed by the following chemical equations.[36]

$$\equiv Si\text{–}OR + H_2O \rightleftharpoons \equiv Si\text{–}OH + ROH \quad (1)$$

$$\equiv Si\text{–}OR + OH\text{–}Si\equiv \rightleftharpoons \equiv Si\text{–}O\text{–}Si\equiv + ROH \quad (2)$$

$$\equiv Si\text{–}OH + OH\text{–}Si\equiv \rightleftharpoons \equiv Si\text{–}O\text{–}Si\equiv + H_2O \quad (3)$$

The forward reaction of eqn (1) shows the hydrolysis of TEOS, and the forward reactions of eqn (2) and (3) demonstrate the polymerization of SiO_2, namely, the growing of the –Si–O–Si– network in $mSiO_2$ silica growth template onto the surfactant molecules.[52] The etching of $mSiO_2$ occurs when the –Si–O–Si– network is destroyed by OH^-, following the three reaction equations in reverse direction. The possible reason

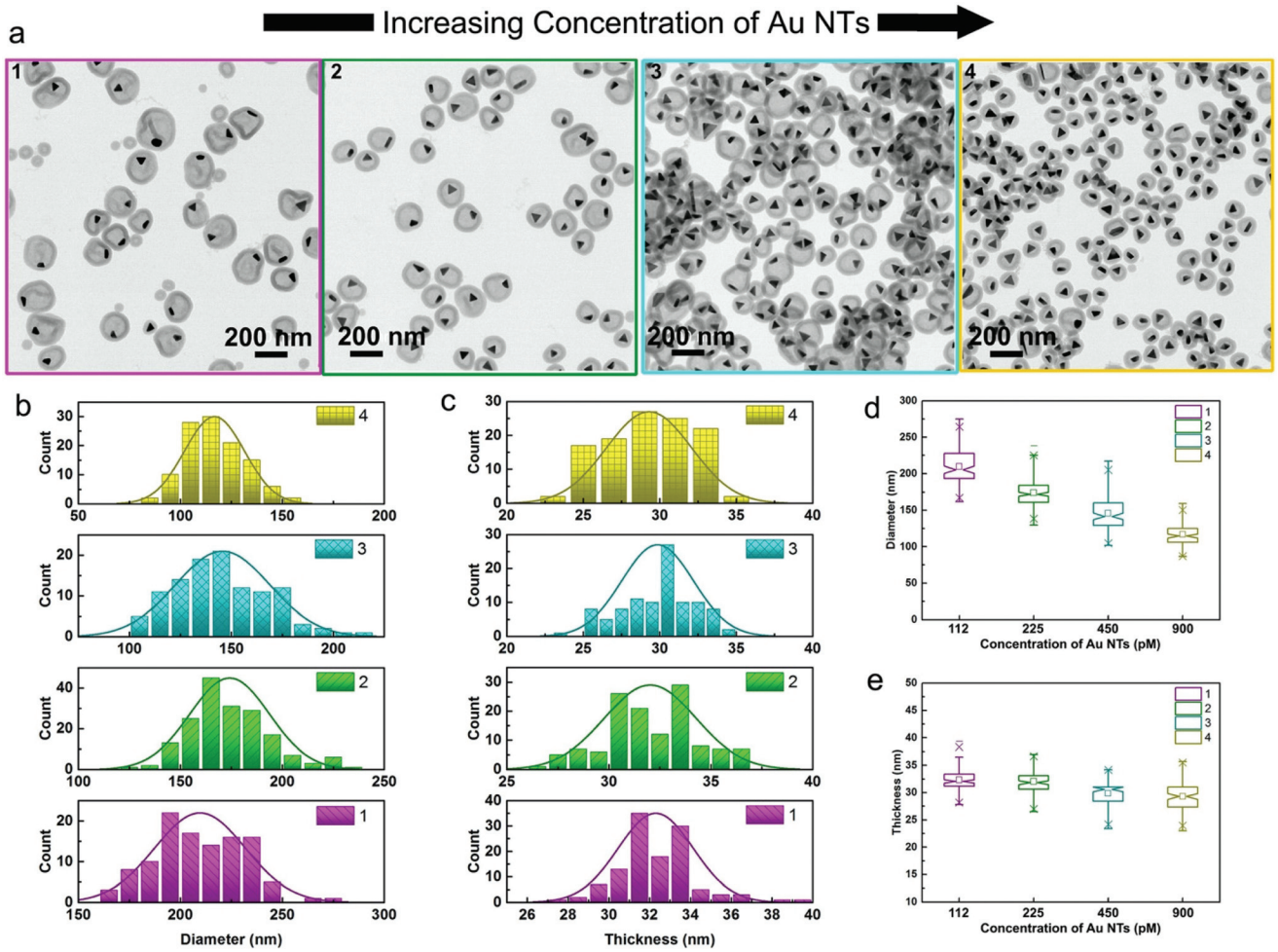

Fig. 3 BF-TEM images and analysis showing the influence of the concentration of Au NTs. In all panels, the magenta, green, cyan, and yellow colors correspond to Au NT concentrations of 112, 225, 450, and 900 pM respectively. (a) TEM images of Au NT@hollow–$mSiO_2$ yolk–shell nanoparticles obtained at the different Au NTs concentrations; (b) histograms of the diameter distribution of Au NT@hollow–$mSiO_2$ yolk–shell nanoparticles; (c) histograms of the shell thickness of Au NT@hollow–$mSiO_2$ yolk–shell nanoparticles; (d) the relationship between the diameter and Au NTs concentrations; (e) the relationship between shell thickness and Au NTs concentrations.

that $mSiO_2$ can be etched from inside out is that the amount of Q2 ($Si(SiO)_2(OX)_2$, X = H or Et) is higher than the amount of Q4 ($Si(SiO)_4$) in the inner part of the $mSiO_2$,[41] as has been found as well for the famous Stöeber process in which ultramicroporous silica particles can be grown[37,40,53,54] while the opposite is the case for the outer part of $mSiO_2$. This makes the etching faster at the interior than at the exterior, and consequently $mSiO_2$ is etched from the inside, finally resulting in the formation of the yolk–shell structure. Our experiments show that reducing the concentration of NaOH for the synthesis leads to the formation of Au NT@$mSiO_2$ core–shell particles instead of hollow particles, also providing evidence that the etching speed of the $mSiO_2$ plays an important role on the formation of yolk–shell particles (Fig. S4†).

The understanding of the growth mechanism as discussed above raises the question of whether the Au NT cores stick on the $mSiO_2$ shell, when the particles remain in solution and/or when the particles are dried and redispersed. To investigate this further, we performed liquid cell TEM (LC-TEM) experiments on the Au NT@hollow–$mSiO_2$ yolk–shell NPs. As shown in ESI Movie S1,† under the imaging condition with a low electron dose rate of 215 e^- nm^{-2} s^{-1}, the Au NT cores did not move at all which means that the Au NTs stick to their $mSiO_2$ shells, because the particles were kept in solution and never dried during the whole experiments since being synthesized. When the electron dose rate was increased to 3940 e^- nm^{-2} s^{-1}, part of the Au NTs in the field of view loosened from their $mSiO_2$ shells and started to move and tumble in the liquid that is also present in between the core and the shells (ESI Movie S2†). The reason that the higher electron dose rate induced the release of the Au NTs is due to the interaction between the electron beam and water, forming OH^- anions by radiolysis, which etch the inner $mSiO_2$ shell and thus released the Au NTs. Thus, mild etching with a NaOH was also observed to obtain freely moving colloids in an outer silica shell as we observed before in previous work.[43,47,55]

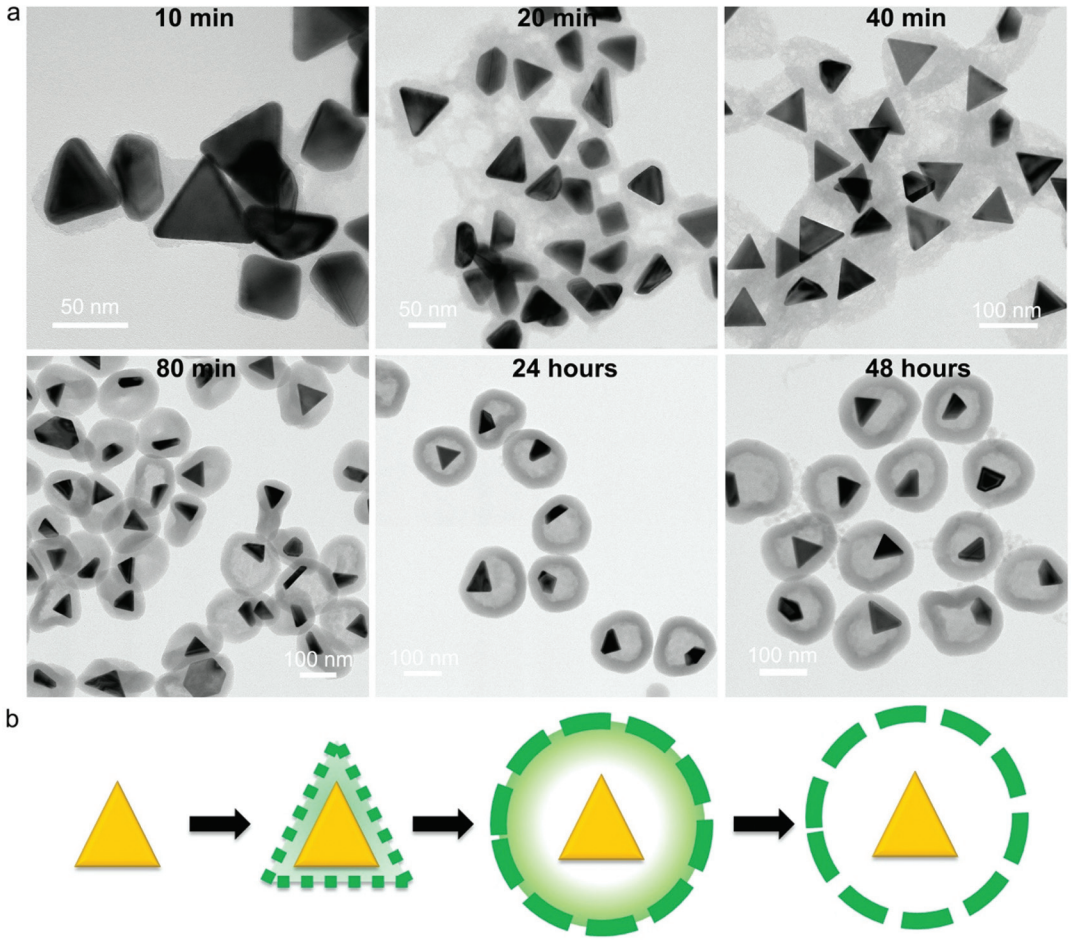

Fig. 4 The growth process of Au NT@hollow–$mSiO_2$ yolk–shell nanoparticles. (a) Evolution in time of the morphology of Au NT@$mSiO_2$ particles at different reaction times in the synthesis. (b) Schematic of the $mSiO_2$ growth-and-etching process.

It is widely known that most nanoparticle synthesis protocols, especially those of NPs, are hard to scale up. Sometimes slightly changing the volume of the growth solution will lead to dramatic changes in the products, especially if a thorough mixing step is part of the synthesis protocol as this is much harder to achieve with larger volumes of a dispersion. With the above understanding of the formation mechanism and influencing factors, the method provided here should be scalable. To verify this, a scaling-up synthesis experiment was performed by enlarging the growth solution to 300 mL which is enlarging it by 30 times compared to the typical syntheses we typically performed. As shown in Fig. S7,† all Au NT@$mSiO_2$ nanoparticles clearly have a yolk–shell structure similarly as was observed for the smaller scale syntheses, showing that the method demonstrated here is up-scalable by at least an order of magnitude.

The localized plasmon resonance property is one of the most attractive features of Au NTs and is sensitive to the local dielectric environment of the metal surface.[56] The main LSPR band of the Au NT@hollow–$mSiO_2$ yolk–shell NPs and Au NT@$mSiO_2$ core–shell NPs was acquired *via* measuring the UV-VIS spectra. In comparison to the Au NTs–CTAC, the LSPR bands of the yolk–shell and core–shell NPs were found to be slightly (~15 nm) red-shifted as shown in Fig. 5, which is attributed to the higher refractive index of the $mSiO_2$ shell with respect to that of H_2O (1.33).[36,44]

With the mechanism proposed above and the finding that other shapes of Au NPs in Au NTs can also form Au NP@$mSiO_2$ yolk–shell structures (Fig. S8a†), and even hollow nanospheres (NSs) (Fig. S8b†), we assume that this synthesis protocol is a core-shape-independent method. To verify our hypothesis, Au nanorods (Au NRs, Fig. 6a) and Au nanocubes (Au NCs, Fig. S9†) were synthesized and used as seeds replacing Au NTs for the synthesis. In line with our expectation, well-defined yolk–shell particles were also formed when using Au NRs and Au NCs as seeds for the synthesis (Fig. 6c and Fig. S10a†).

Moreover, even without using any Au NPs as seeds, hollow $mSiO_2$ NSs were still obtained (Fig. S10b†). In addition, both Au NR@$mSiO_2$ core–shell and yolk–shell particles can be acquired by simply tuning the concentration of the Au NRs (Fig. 6b and c), which further corroborates our findings on the influence of the concentration of the Au NTs. The LSPR band of Au NRs with and without $mSiO_2$ are shown in Fig. 6d, and

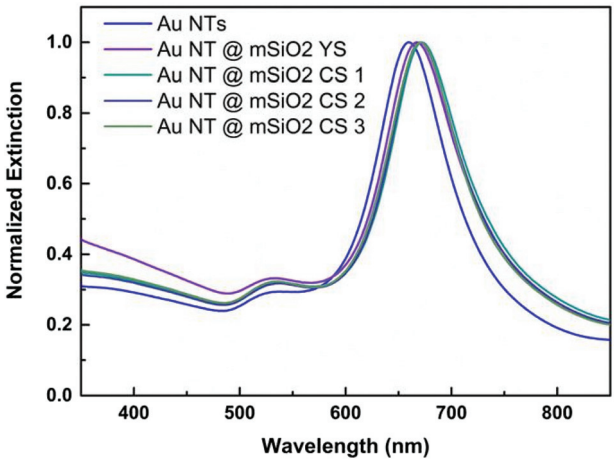

Fig. 5 UV-VIS spectrum of Au NT@mSiO$_2$ NPs with hollow 'yolk–shell' or core–shell morphology. The particles were synthesized using following conditions: the concentrations of TEOS precursor solution used for the reaction were: (YS) 20 vol%, (CS 1) 15 vol%, (CS 2) 10 vol%, and (CS 3) 5 vol%.

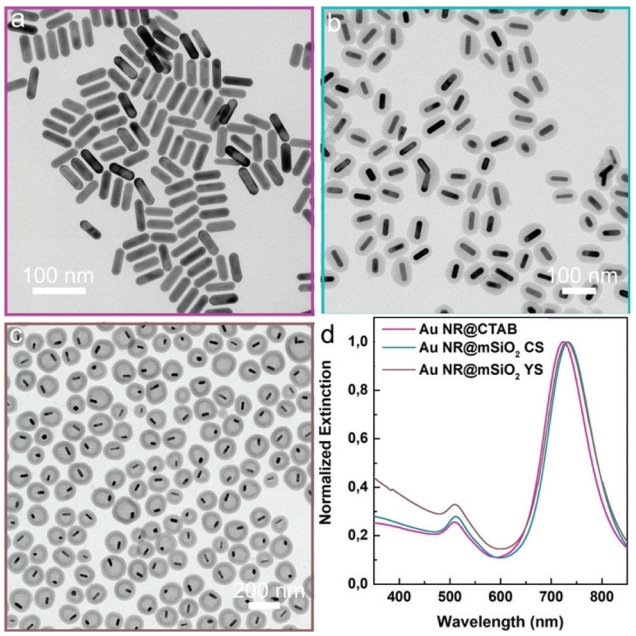

Fig. 6 (a) BF-TEM image of Au NRs, (b) BF-TEM image of Au NR@mSiO$_2$ core–shell NPs, (c) BF-TEM image of Au NR@hollow–mSiO$_2$ yolk–shell NPs, and (d) UV-VIS spectra of Au NR, Au NR@mSiO$_2$ core–shell and yolk–shell NPs.

similarly to the case of the Au NTs, the mSiO$_2$ shells caused the LSPR bands of Au NRs to be slightly red-shifted in comparison to Au NR–CTAB. Lastly, the synthesis method demonstrated here was proven to be equally applicable for preparing Au NT@M (Ag, Pd, & Pt)@hollow–mSiO$_2$ yolk–shell NPs (Fig. S11–S14†). Thus, it is safe to conclude that the method will work well for synthesizing yolk–shell NPs of mSiO$_2$ and other metal NPs, as long as the metal surface is protected by CTAC or CTAB molecules and it is even likely that also other NPs, as long as their ligands can be replaced with CTAB/CTAC can be used as cores as well.

Conclusions

In summary, we have developed a scalable single-step coating method for the synthesis of Au NP@hollow–mSiO$_2$ yolk–shell structures. It features a single-step coating, using CTAB or CTAC as pore inducing agent and its suitability for various shapes of Au NPs, tunability of the hollow space between the core and the shell, and opportunity for scaled-up synthesis have been demonstrated. In addition, we showed that the Au NP@hollow–mSiO$_2$ yolk–shell structure forms *via* a growth-etching synergistic mechanism that was revealed by time-resolved TEM images. Compared to the LSPR band of Au NT–CATC, the LSPR bands of Au NT@mSiO$_2$ core–shell particles and Au NT@hollow–mSiO$_2$ particles show a slight red shift and mild etching allows the metal NPs to be freely diffusing in the mesoporous silica shell. Considering the generality of this method, it can very likely also be used for synthesizing mSiO$_2$ based shell yolk–shell particles for other kinds of NPs cores, *e.g.*, semiconductors quantum dots, upconversion rare earth doped NPs, and metallic oxide NPs. As such, this versatile synthesis method of yolk–shell particles helps realizing applications of these NPs in catalysis, targeted drug delivery, *in vivo* imaging, and sensing.

Experimental

Synthetic procedures of Au NT@mSiO$_2$

A volume of 10 mL of Au NTs storage solution was centrifuged at 9000 rpm for 10 minutes. After centrifuging, the suspension was removed and the sediment was suspended in 10 mL of deionized water and transferred into a 20 mL glass vial. 150 μL of 0.1 M CATC and 100 μL of 0.10 M NaOH were added into above Au NTs solution. Lastly, 200 μL of 20 vol% TEOS in methanol was injected into the above solution in one shot under stirring. The solution was stirred for 45–48 hours. More details of changing the reaction conditions synthesis and their corresponding figures are shown in Table S1 in ESI.†

More details of Experimental section, *e.g.* chemicals, characterization, and liquid-cell TEM experiments, can be found in ESI.†

Conflicts of interest

There are no conflicts to declare.

Acknowledgements

We thank Dr Da Wang for the useful discussions. X. X. and A. v. B. acknowledge financial support from EU H2020-

MSCA-ITN-2015 project 'MULTIMAT' (project number: 676045). M. v. H. acknowledges the European Research Council for an ERC-CoG grant (NANO-INSITU, grant no. 683076).

References

1 C. Boerigter, R. Campana, M. Morabito and S. Linic, *Nat. Commun.*, 2016, **7**, 10545.
2 Z. Bian, T. Tachikawa, P. Zhang, M. Fujitsuka and T. Majima, *J. Am. Chem. Soc.*, 2014, **136**, 458–465.
3 Y. C. Tsao, S. Rej, C. Y. Chiu and M. H. Huang, *J. Am. Chem. Soc.*, 2014, **136**, 396–404.
4 M. Dunwell, Q. Lu, J. M. Heyes, J. Rosen, J. G. Chen, Y. Yan, F. Jiao and B. Xu, *J. Am. Chem. Soc.*, 2017, **139**, 3774–3783.
5 J. Duan, L. Bai, K. Xu, Q. Fang, Y. Sun, H. Xu, K. C. Leung and S. Xuan, *J. Hazard. Mater.*, 2020, **15**, 121276.
6 X. Zhu, H. K. Yip, X. Zhuo, R. Jiang, J. Chen, X. M. Zhu, Z. Yang and J. Wang, *J. Am. Chem. Soc.*, 2017, **139**, 13837–13846.
7 G. Bodelon, V. Montes-Garcia, V. Lopez-Puente, E. H. Hill, C. Hamon, M. N. Sanz-Ortiz, S. Rodal-Cedeira, C. Costas, S. Celiksoy, I. Perez-Juste, L. Scarabelli, A. La Porta, J. Perez-Juste, I. Pastoriza-Santos and L. M. Liz-Marzan, *Nat. Mater.*, 2016, **15**, 1203–1211.
8 Y. Liu, Z. Wang, Y. Liu, G. Zhu, O. Jacobson, X. Fu, R. Bai, X. Lin, N. Lu, X. Yang, W. Fan, J. Song, Z. Wang, G. Yu, F. Zhang, H. Kalish, G. Niu, Z. Nie and X. Chen, *ACS Nano*, 2017, **11**, 10539–10548.
9 Y. Zhao, Y. Huang, H. Zhu, Q. Zhu and Y. Xia, *J. Am. Chem. Soc.*, 2016, **138**, 16645–16654.
10 P. Li, Y. Li, Z. K. Zhou, S. Tang, X. F. Yu, S. Xiao, Z. Wu, Q. Xiao, Y. Zhao, H. Wang and P. K. Chu, *Adv. Mater.*, 2016, **28**, 2511–2517.
11 H. Jing, Q. Zhang, N. Large, C. Yu, D. A. Blom, P. Nordlander and H. Wang, *Nano Lett.*, 2014, **14**, 3674–3682.
12 S. Schlucker, *Angew. Chem., Int. Ed.*, 2014, **53**, 4756–4795.
13 S.-Y. Ding, J. Yi, J.-F. Li, B. Ren, D.-Y. Wu, R. Panneerselvam and Z.-Q. Tian, *Nat. Rev. Mater.*, 2016, **1**, 16021.
14 X. Xie, G. Gao, S. Kang, Y. Lei, Z. Pan, T. Shibayama and L. Cai, *Nanotechnology*, 2017, **28**, 245602.
15 H. Huang, L. Zhang, Z. Lv, R. Long, C. Zhang, Y. Lin, K. Wei, C. Wang, L. Chen, Z. Y. Li, Q. Zhang, Y. Luo and Y. Xiong, *J. Am. Chem. Soc.*, 2016, **138**, 6822–6828.
16 D. Andren, L. Shao, N. Odebo Lank, S. S. Acimovic, P. Johansson and M. Kall, *ACS Nano*, 2017, **11**, 10053–10061.
17 H. A. Atwater and A. Polman, *Nat. Mater.*, 2010, **9**, 205–213.
18 X. Huang, Y. Li, Y. Chen, H. Zhou, X. Duan and Y. Huang, *Angew. Chem., Int. Ed.*, 2013, **52**, 6063–6067.
19 S. Linic, U. Aslam, C. Boerigter and M. Morabito, *Nat. Mater.*, 2015, **14**, 567–576.
20 M. L. Personick and C. A. Mirkin, *J. Am. Chem. Soc.*, 2013, **135**, 18238–18247.
21 Y. Xia, X. Xia and H. C. Peng, *J. Am. Chem. Soc.*, 2015, **137**, 7947–7966.
22 Q. Zhang, Y. Zhou, E. Villarreal, Y. Lin, S. Zou and H. Wang, *Nano Lett.*, 2015, **15**, 4161–4169.
23 L. Polavarapu, D. Zanaga, T. Altantzis, S. Rodal-Cedeira, I. Pastoriza-Santos, J. Perez-Juste, S. Bals and L. M. Liz-Marzan, *J. Am. Chem. Soc.*, 2016, **138**, 11453–11456.
24 X. Xie, G. Gao, S. Kang, T. Shibayama, Y. Lei, D. Gao and L. Cai, *Adv. Mater.*, 2015, **27**, 5573–5577.
25 X. Xie, M. A. van Huis and A. van Blaaderen, *Nanoscale*, 2021, **13**, 2902–2913.
26 W. Albrecht, T. S. Deng, B. Goris, M. A. van Huis, S. Bals and A. van Blaaderen, *Nano Lett.*, 2016, **16**, 1818–1825.
27 Y. Bai, C. Gao and Y. Yin, *Nanoscale*, 2017, **9**, 14875–14880.
28 A. Guerrero-Martinez, J. Perez-Juste and L. M. Liz-Marzan, *Adv. Mater.*, 2010, **22**, 1182–1195.
29 S. H. Joo, J. Y. Park, C. K. Tsung, Y. Yamada, P. Yang and G. A. Somorjai, *Nat. Mater.*, 2009, **8**, 126–131.
30 Z. Teng, W. Li, Y. Tang, A. Elzatahry, G. Lu and D. Zhao, *Adv. Mater.*, 2019, **31**, 1707612–1707636.
31 I. Gorelikov and N. Matsuura, *Nano Lett.*, 2008, **8**, 369–373.
32 W. Zhu, Z. Chen, Y. Pan, R. Dai, Y. Wu, Z. Zhuang, D. Wang, Q. Peng, C. Chen and Y. Li, *Adv. Mater.*, 2019, **31**, 1800426–1800456.
33 Z. Wang, Z. M. Chang, D. Shao, F. Zhang, F. Chen, L. Li, M. F. Ge, R. Hu, X. Zheng, Y. Wang and W. F. Dong, *ACS Appl. Mater. Interfaces*, 2019, **11**(38), 34755–34765.
34 B. Li and H. C. Zeng, *Adv. Mater.*, 2019, **31**, 1801104–1801132.
35 D. Mao, J. Wan, J. Wang and D. Wang, *Adv. Mater.*, 2019, **31**, 1802874–1802893.
36 L. R. Rowe, B. S. Chapman and J. B. Tracy, *Chem. Mater.*, 2018, **30**, 6249–6258.
37 Y. Chen, H. R. Chen and J. L. Shi, *Acc. Chem. Res.*, 2014, **47**, 125–137.
38 X. W. D. Lou, L. A. Archer and Z. Yang, *Adv. Mater.*, 2008, **20**, 3987–4019.
39 Y. Si, M. Chen and L. Wu, *Chem. Soc. Rev.*, 2016, **45**, 690–714.
40 X. Wang, J. Feng, Y. Bai, Q. Zhang and Y. Yin, *Chem. Rev.*, 2016, **116**, 10983–11060.
41 Z. Teng, S. Wang, X. Su, G. Chen, Y. Liu, Z. Luo, W. Luo, Y. Tang, H. Ju, D. Zhao and G. Lu, *Adv. Mater.*, 2014, **26**, 3741–3747.
42 A. A. Volkert, M. C. S. Pierre, B. Shrestha and A. J. Haes, *RSC Adv.*, 2015, **5**, 3774–3780.
43 K. Watanabe, T. A. J. Welling, S. Sadighikia, H. Ishii, A. Imhof, M. A. van Huis, A. van Blaaderen and D. Nagao, *J. Colloid Interface Sci.*, 2020, **566**, 202–210.
44 T.-S. Deng, J. E. S. van der Hoeven, A. O. Yalcin, H. W. Zandbergen, M. A. van Huis and A. van Blaaderen, *Chem. Mater.*, 2015, **27**, 7196–7203.
45 M. Priebe and K. M. Fromm, *Chem. – Eur. J.*, 2015, **21**, 3854–3874.

46 Q. Fan, H. Yang, J. Ge, S. Zhang, Z. Liu, B. Lei, T. Cheng, Y. Li, Y. Yin and C. Gao, *Research*, 2020, **2020**, 2131806.
47 D. Nagao, C. M. van Kats, K. Hayasaka, M. Sugimoto, M. Konno, A. Imhof and A. van Blaaderen, *Langmuir*, 2010, **26**, 5208–5212.
48 L. Scarabelli, M. Coronado-Puchau, J. J. Giner-Casares, J. Langer and L. M. Liz-Marzán, *ACS Nano*, 2014, **8**, 5833–5842.
49 D. Shen, J. Yang, X. Li, L. Zhou, R. Zhang, W. Li, L. Chen, R. Wang, F. Zhang and D. Zhao, *Nano Lett.*, 2014, **14**, 923–932.
50 A. M. Vinogradov, A. S. Tatikolov and S. M. B. Costa, *Phys. Chem. Chem. Phys.*, 2001, **3**, 4325–4332.
51 B. Thierry, J. Ng, T. Krieg and H. J. Griesser, *Chem. Commun.*, 2009, 1724–1726.
52 P. Selvam, S. K. Bhatia and C. G. Sonwane, *Ind. Eng. Chem. Res.*, 2001, **40**, 3237–3261.
53 Y. Han, Z. Guo, S. Teng, H. Xia, D. Wang, M.-Y. Han and W. Yang, *Chem. Mater.*, 2019, **31**(18), 7470–7477.
54 Y. J. Wong, L. Zhu, W. S. Teo, Y. W. Tan, Y. Yang, C. Wang and H. Chen, *J. Am. Chem. Soc.*, 2011, **133**, 11422–11425.
55 K. Watanabe, H. Ishii, M. Konno, A. Imhof, A. van Blaaderen and D. Nagao, *Langmuir*, 2017, **33**, 296–302.
56 H. Chen, M. Tian, L. Zhao, F. Wang, L. Sun, J. Wang and C. Yan, *Nano Today*, 2010, 494–505.